

High-fidelity universal quantum gates for hybrid systems via the practical photon scattering

Jun-Wen Luo(罗俊文) and Guan-Yu Wang(王冠玉)[†]

College of Mathematics and Physics, Beijing University of Chemical Technology, Beijing 100029, China

(Received 29 May 2022; revised manuscript received 22 July 2022; accepted manuscript online 5 August 2022)

High-fidelity quantum logic gates are essential in quantum computation, and both photons and electron spins in quantum dots (QDs) have their own unique advantages in implementing quantum computation. It is of critical significance to achieve high-fidelity quantum gates for photon-QD hybrid systems. Here, we propose two schemes for implementing high-fidelity universal quantum gates including Toffoli gate and Fredkin gate for photon-QD hybrid systems, utilizing the practical scattering of a single photon off a QD-cavity system. The computation errors from the imperfections involved in the practical scattering are detected and prevented from arising in the final results of the two gates. Accordingly, the unity fidelity of each quantum gate is obtained in the nearly realistic condition, and the requirement for experimental realization is relaxed. Furthermore, the quantum circuits for the two gates are compact and no auxiliary qubits are required, which would also be the advantages regarding their experimental feasibility. These features indicate that our schemes may be useful in the practical quantum computation tasks.

Keywords: quantum computation, quantum dot, photon, microcavity

PACS: 03.67.Lx, 03.67.Pp

DOI: [10.1088/1674-1056/ac8734](https://doi.org/10.1088/1674-1056/ac8734)

1. Introduction

Quantum information processing (QIP) is accomplished based on quantum mechanics and can surpass classical devices in terms of speed, efficiency, and security.^[1] Quantum computation, one of the most important branches of QIP tasks, can use superposition to achieve evaluating a function $f(x)$ for many different values of x simultaneously rather than sequentially, which is parallel computing.^[1] Quantum computation utilizing its capability of parallel exhibits a fascinating performance, such as largely speeding up large number factorization^[2] and unsorted database search.^[3,4] The ultimate aim of quantum computation is realizing quantum computers, and the key elements in quantum computers are quantum logic gates. Many investigations have been focused on the two-qubit controlled-NOT (CNOT) gate or its identical controlled-phase-flip (CPF) gate.^[5,6] In the domain of three-qubit gates, Toffoli and Fredkin gates have attracted much attention and both of them are universal quantum gates. Together with Hadamard gates, they can realize unitary manipulation for a multi-qubit system.^[7,8] Moreover, they are critical in phase estimation,^[1] complex quantum algorithms,^[2-4] error correction,^[9] and fault tolerant quantum circuits.^[10]

Nowadays, quantum logic gates have been implemented with many physical systems, which can be classified into moving systems and stationary systems. Photon is a natural flying physical architecture and an ideal candidate as an information carrier for its high transmitting speed, weak interaction with the environment, and easy and accurate manipulation. By far, many efforts have been made to implement

ing quantum gates utilizing photonic system in one degree of freedom (DOF) or multiple DOFs.^[11-23] Stationary systems are suitable for processor and local storage, and several stationary systems have been used to implement quantum gates, such as nuclear magnetic resonance,^[24-27] superconducting qubits,^[28-33] quantum dots (QDs),^[34-38] diamond nitrogen-vacancy (NV) centers,^[39-41] and atoms or ions.^[42-48] Hybrid systems composed of flying photons and stationary systems allow exploiting different physical systems at the best of their potentials,^[49] and the quantum gates for hybrid systems hold a great promise for quantum communication and computation, especially for quantum repeaters, distributed quantum computation, and blind quantum computation. Some interesting schemes of quantum gates for hybrid systems have been proposed. For example, in 2005, Liang and Li^[50] proposed a theoretical scheme of a two-qubit SWAP gate on a photon and a trapped atom or ion. In 2013, Wei and Deng^[51] proposed some schemes for universal hybrid quantum gates. In 2014, Reiserer *et al.*^[5] realized a quantum CPF gate between a flying photon and a single trapped atom in experiment. In the same year, Wang *et al.*^[52] proposed some interesting schemes for universal hybrid hyper-controlled quantum gates. In 2018, Bechler *et al.*^[53] demonstrated the experiment to achieve the photon-atom qubit swap operation. Recently, Song *et al.*^[54] constructed heralded quantum gates for hybrid systems.

Trapping atoms or artificial atoms (such as QD, superconductor, diamond NV center, Josephson junction) in microcavities forms an attractive stationary system since cavity quantum electrodynamics (QED) can enhance the inter-

[†]Corresponding author. E-mail: wangguanyu@buct.edu.cn

© 2023 Chinese Physical Society and IOP Publishing Ltd

action between a single photon and an (artificial) atom. The electron spin in a GaAs-based or InAs-based charged QD trapped in a microcavity has attracted much attention. The electron spin in a charged QD owns long coherence time, which can maintain 3 μ s,^[55,56] and its relaxation time can reach the order of ms^[57,58] through the spin-echo technique. Meanwhile, fast preparation of the superposition state of the electron spin,^[59,60] fast manipulation,^[61–64] and detection of the electron spin state^[65] have been demonstrated. Furthermore, researchers have realized embedding a QD in a microcavity,^[66,67] and the interaction between a photon and a QD trapped in a cavity.^[68,69] The scattering of a single photon off a cavity with a QD is viewed as a promising platform for implementing universal quantum gates,^[70] and it has been used to realize a QD photon-sorter^[71] and a spin-photon quantum phase switch.^[72]

Under the ideal scattering condition, the photon will be perfectly reflected or transmitted by the (artificial) atom-cavity system depending on the state of the photon and that of the (artificial) atom, and the desired result of the quantum gate can be obtained via this perfect photon scattering. However, when it turns into realistic condition, the practical scattering becomes imperfect, which would lead to computation errors appearing in the result of the quantum gate in company with the reduced fidelity^[73] and may accordingly reduce the quality of the entanglement distillation accomplished with quantum gates.^[74,75] That is to say, the performance of the quantum gates is restricted by the realistic condition such as coupling strength, cavity leakage and frequency difference. For improving the performance of quantum gates in the realistic condition and relaxing the requirement for experiment, it is worthy to seek ways for implementing quantum gates working with fewer computation errors and higher fidelity in the realistic condition via different methods.^[73,76–91]

Resorting to the practical scattering of a single photon off a QD-cavity system, we present two schemes for implementing high-fidelity universal quantum gates including Toffoli gate and Fredkin gate for photon-QD hybrid systems. In the Toffoli gate, the flying photon and the electron spin in the QD act as control qubits and the electron spin in the other QD acts as the target qubit, and in the Fredkin gate the flying photon and two electron spins in the QDs respectively act as the control qubit and the target qubits. The imperfect scattering arising from the realistic condition such as weak coupling strength, cavity leakage, and frequency difference is taken into account in our schemes, and the computation errors from the imperfect scattering are detected and prevented from appearing in the final result of the two gates. Accordingly, the fidelity of each quantum gate is robust to the realistic parameters of practical scattering, and the requirement for its experimental realization is relaxed. Meanwhile, these two schemes are im-

plemented without auxiliary qubits, which further improves the experimental feasibility. These interesting features may make our schemes more useful in practical quantum computation tasks.

2. The practical scattering of the photon off the QD embedded in a double-sided microcavity

We consider a singly charged electron In(Ga)As QD or a GaAs interface QD embedded in an optical resonant double-sided microcavity with two of the same mirrors partially reflective in the top and the bottom, as shown in Fig. 1(a). When an excess electron is injected into a QD, optical excitation can create a negatively charged exciton X^- , which is composed of two electrons bound to one heavy hole. There are two kinds of optical transitions between the exciton X^- and the electron. The polarized photon with spin $s_z = +1$ ($|L^\downarrow\rangle$ or $|R^\uparrow\rangle$) couples to the optical transition $|\uparrow\rangle \leftrightarrow |\uparrow\downarrow\uparrow\rangle$, and the polarized photon with spin $s_z = -1$ ($|R^\downarrow\rangle$ or $|L^\uparrow\rangle$) couples to the optical transition $|\downarrow\rangle \leftrightarrow |\downarrow\uparrow\downarrow\rangle$, as shown in Fig. 1(b). Here, $|\uparrow\rangle$ and $|\downarrow\rangle$ represent the states of the excess electron spin in a QD with projections $\pm 1/2$ along the quantization axis (z direction); $|\uparrow\downarrow\uparrow\rangle$ and $|\downarrow\uparrow\downarrow\rangle$ denote the states of the exciton, where $|\uparrow\rangle$ and $|\downarrow\rangle$ are the heavy-hole states with projections $\pm 3/2$ along the quantization axis, respectively. $|R\rangle$ and $|L\rangle$ represent the states of the right- and left-circularly polarized photon, respectively, and the superscript arrows \uparrow and \downarrow indicate the photon propagating along and against the quantization axis, respectively.

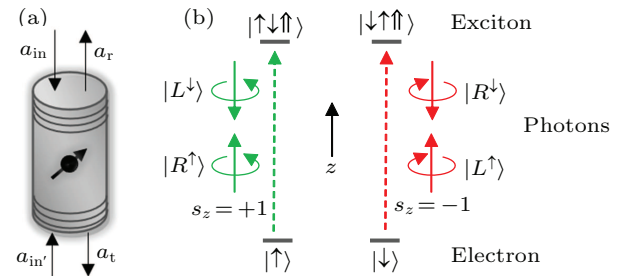


Fig. 1. (a) Schematic diagram for an electron spin in a QD embedded in an optical resonant double-sided microcavity. (b) Schematic description of the relevant exciton energy levels and the spin selection rules for dipole transitions of negatively charged excitons. The optical transitions $|\uparrow\rangle \leftrightarrow |\uparrow\downarrow\uparrow\rangle$ and $|\downarrow\rangle \leftrightarrow |\downarrow\uparrow\downarrow\rangle$ are resonantly coupled to the polarized photons with $s_z = +1$ ($|L^\downarrow\rangle$ or $|R^\uparrow\rangle$) and $s_z = -1$ ($|R^\downarrow\rangle$ or $|L^\uparrow\rangle$), respectively.

The process of a single-photon scattering off a QD-cavity system can be represented by the Heisenberg equations of motion for the cavity field operator \hat{a} and the dipole operator $\hat{\sigma}_-$ along with the input-output relations^[92]

$$\begin{aligned} \frac{d\hat{a}}{dt} &= -\left[i(\omega_c - \omega) + \kappa + \frac{\kappa_s}{2}\right]\hat{a} - g\hat{\sigma}_- \\ &\quad - \sqrt{\kappa}(\hat{a}_{in'} + \hat{a}_{in}) + \hat{H}, \\ \frac{d\hat{\sigma}_-}{dt} &= -\left[i(\omega_{X^-} - \omega) + \frac{\gamma}{2}\right]\hat{\sigma}_- - g\hat{\sigma}_z\hat{a} + \hat{G}, \end{aligned}$$

$$\begin{aligned}\hat{a}_r &= \hat{a}_{in} + \sqrt{\kappa} \hat{a}, \\ \hat{a}_t &= \hat{a}_{in'} + \sqrt{\kappa} \hat{a},\end{aligned}\quad (1)$$

where \hat{a}_{in} , $\hat{a}_{in'}$, \hat{a}_r , and \hat{a}_t are the input and output field operators; g is the coupling strength between the electron X^- and the microcavity; ω , ω_c , and ω_{X^-} are frequencies of the photon, the microcavity, and the X^- transition, respectively; γ , κ , and κ_s represent the X^- dipole decay rate, the microcavity decay rate, and the microcavity leaky rate, respectively; \hat{H} and \hat{G} are noise operators.

In the limit of a weak incoming field, the charged QD is predominantly in the ground state in the whole process, that is, $\langle \hat{\sigma}_z \rangle \approx -1$. The reflection coefficient $r(\omega)$ and the transmission coefficient $t(\omega)$ of the single-photon scattering off a QD-cavity system can be expressed as^[70,93]

$$\begin{aligned}r(\omega) &= 1 + t(\omega), \\ t(\omega) &= -\frac{-\kappa[i(\omega_{X^-} - \omega) + \frac{\gamma}{2}]}{[i(\omega_{X^-} - \omega) + \frac{\gamma}{2}][i(\omega_c - \omega) + \kappa + \frac{\kappa_s}{2}] + g^2}.\end{aligned}\quad (2)$$

When the circularly polarized photon is scattered off a cold microcavity, that is, the photon is uncoupled to the dipole transition (i.e., $g = 0$), the specific reflection and transmission coefficients can be simplified to

$$\begin{aligned}r_0(\omega) &= 1 + t_0(\omega), \\ t_0(\omega) &= -\frac{\kappa}{i(\omega_c - \omega) + \kappa + \frac{\kappa_s}{2}}.\end{aligned}\quad (3)$$

Here, the reflection and transmission coefficients are the functions of the realistic parameters of the practical scattering, such as the coupling strength $g/(2\kappa + \kappa_s)$, cavity leakage κ_s/κ , and the frequency difference $\Delta = \omega - \omega_c$. Therefore, the evolution rules for the practical scattering of the photon off the QD-cavity system can be detailedly written as

$$\begin{aligned}|R^\uparrow \uparrow\rangle &\rightarrow r(\omega) |L^\downarrow \uparrow\rangle + t(\omega) |R^\uparrow \uparrow\rangle, \\ |L^\downarrow \uparrow\rangle &\rightarrow r(\omega) |R^\uparrow \uparrow\rangle + t(\omega) |L^\downarrow \uparrow\rangle, \\ |R^\downarrow \uparrow\rangle &\rightarrow t_0(\omega) |R^\downarrow \uparrow\rangle + r_0(\omega) |L^\uparrow \uparrow\rangle, \\ |L^\uparrow \uparrow\rangle &\rightarrow t_0(\omega) |L^\uparrow \downarrow\rangle + r_0(\omega) |R^\downarrow \uparrow\rangle, \\ |R^\downarrow \downarrow\rangle &\rightarrow r(\omega) |L^\uparrow \downarrow\rangle + t(\omega) |R^\downarrow \downarrow\rangle, \\ |L^\uparrow \downarrow\rangle &\rightarrow r(\omega) |R^\downarrow \downarrow\rangle + t(\omega) |L^\uparrow \downarrow\rangle, \\ |R^\uparrow \downarrow\rangle &\rightarrow t_0(\omega) |R^\uparrow \downarrow\rangle + r_0(\omega) |L^\downarrow \downarrow\rangle, \\ |L^\downarrow \downarrow\rangle &\rightarrow t_0(\omega) |L^\downarrow \downarrow\rangle + r_0(\omega) |R^\uparrow \downarrow\rangle.\end{aligned}\quad (4)$$

3. High-fidelity Toffoli gate on a three-qubit hybrid system

A Toffoli gate on a three-qubit hybrid system is used to perform a NOT operation on a target qubit (encoded on an electron spin in a QD) or not, depending on the states of the control qubits (respectively encoded on a flying photon and an

electron spin in the other QD). For obtaining the Toffoli gate without computation errors coming from the imperfect scattering (i.e., obtaining the Toffoli gate with a high fidelity robust to the realistic parameters of the practical scattering), we let the circularly polarized photon interact with the basic block based on the practical scattering off the QD-cavity system.

The basic block is shown in the inset of Fig. 2. Here, TR is an optical switch, which can be controlled exactly as needed to reflect or transmit a photon. BS is a 50:50 beam splitter completing a Hadamard operation $[|i_1\rangle \rightarrow \frac{1}{\sqrt{2}}(|j_1\rangle + |j_2\rangle), |i_2\rangle \rightarrow \frac{1}{\sqrt{2}}(|j_1\rangle - |j_2\rangle)]$ on the spatial-mode DOF of a photon. HWP represents a half-wave plate performing a Hadamard operation $[|R\rangle \rightarrow \frac{1}{\sqrt{2}}(|R\rangle + |L\rangle), |L\rangle \rightarrow \frac{1}{\sqrt{2}}(|R\rangle - |L\rangle)]$ on the polarization DOF of a photon. R is a fully reflective mirror and D is a single-photon detector. Suppose that the injected photon is in the right-polarization state $|R\rangle$, and the electron spin in the QD is initially prepared in the arbitrary normalized state $|\phi_s\rangle = \alpha|\uparrow\rangle + \beta|\downarrow\rangle$. After the injected photon being transmitted by the TR and experiencing the Hadamard operations in the spatial-mode and polarization DOFs respectively by the BS and HWPs, it interacts with the QD-cavity system according to the rules for the practical scattering of the photon off the QD-cavity system as described in Eq. (4). Then the photon passes through the HWPs and BS again, and the final state of the system composed of the photon and the electron spin in the QD becomes^[94]

$$|\Phi\rangle_1 = D|R\rangle_{i_1}(\alpha|\uparrow\rangle + \beta|\downarrow\rangle) + T|L\rangle_{i_2}(\alpha|\uparrow\rangle - \beta|\downarrow\rangle), \quad (5)$$

where $D = \frac{1}{2}(t + r + t_0 + r_0)$ and $T = \frac{1}{2}(t + r - t_0 - r_0)$ are the reflection and transmission coefficients of the basic block, respectively. The first term of the Eq. (5) corresponds to the termination of the following process. In this case, the photon is reflected out of the basic block by TR with the probability of $|D|^2$ and then triggers the single-photon detector, and the polarization state of the photon and the state of the electron spin in the QD would not be changed. Conversely, the second term of the Eq. (5) corresponds to the desired outcome, where the photon is transmitted out of the basic block from path i_2 to the following circuit with the probability of $|T|^2$. Accordingly, the polarization of the photon is flipped from $|R\rangle$ to $|L\rangle$, and the state of the electron spin in the QD is changed from $|\phi_s\rangle$ to $|\phi'_s\rangle = \alpha|\uparrow\rangle - \beta|\downarrow\rangle$.

Utilizing the optical elements and the basic blocks, we propose the scheme for our high-fidelity Toffoli gate on a three-qubit hybrid system. Suppose that the control photon, the control electron spin in QD₁, and the target electron spin in QD₂ are prepared in arbitrary normalized states $|\psi\rangle_p$, $|\psi\rangle_{e_1}$, and $|\psi\rangle_{e_2}$, respectively, where

$$\begin{aligned}|\psi\rangle_p &= \alpha_p|R\rangle + \beta_p|L\rangle, \\ |\psi\rangle_{e_1} &= \alpha_{e_1}|\uparrow\rangle_1 + \beta_{e_1}|\downarrow\rangle_1, \\ |\psi\rangle_{e_2} &= \alpha_{e_2}|\uparrow\rangle_2 + \beta_{e_2}|\downarrow\rangle_2.\end{aligned}\quad (6)$$

The Toffoli gate completes the task that when the control photon and the control electron spin in QD₁ are in the states $|L\rangle$ and $|\downarrow\rangle$, respectively, the state of the target electron spin in QD₂ is flipped; otherwise, the state of the target electron spin is unchanged. The quantum circuit for the high-fidelity Toffoli gate is shown in Fig. 2. Here, CPBS is a circularly polarizing beam splitter which transmits the right-circularly polarized photon component $|R\rangle$ and reflects the left-circularly polarized photon component $|L\rangle$. WFC denotes a wave-form corrector which can modify the intensity of the photon passing through it with a coefficient, and it can be achieved by employing an unbalanced beam splitter.^[95,96] WFC₁ and WFC_{2,3,4} introduce coefficients T^3 and T , respectively, on the photon. QWP represents a quarter-wave plate realizing the polarization bit-flip operation $\sigma_x = |R\rangle\langle L| + |L\rangle\langle R|$ on a photon. P_π is a phase shifter contributing a π shift to the incident photon. The detailed principle of the high-fidelity Toffoli gate is given in the following.

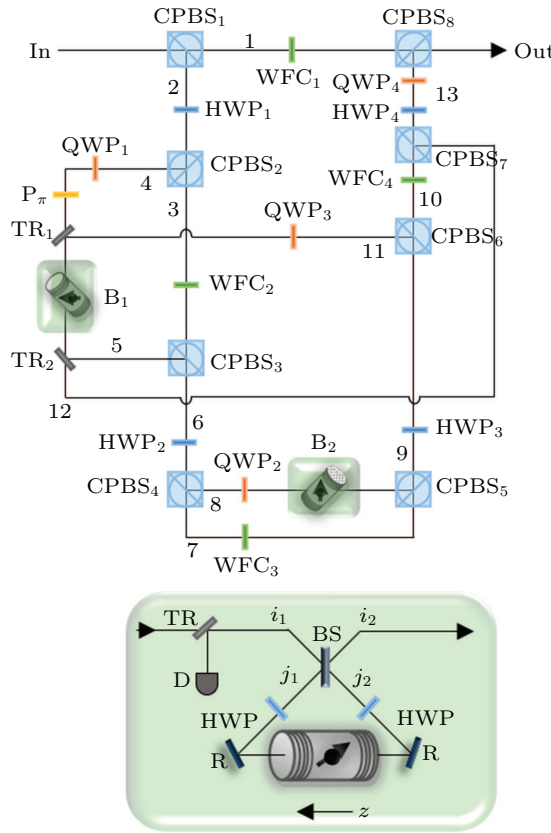


Fig. 2. Schematic diagram for the high-fidelity Toffoli gate on a three-qubit hybrid system. Here, CPBS is a circularly polarizing beam splitter. WFC denotes a wave-form corrector and WFC₁ and WFC_{2,3,4} modify the intensity of the incident photon with coefficients T^3 and T , respectively. HWP represents a half-wave plate, QWP represents a quarter-wave plate, P_π denotes a phase shifter, and TR is an optical switch. B represents a basic block consisting of QD-microcavity system as shown in the inset, in which BS is a 50:50 beam splitter, R is a fully reflective mirror, and D is a single-photon detector.

First, the injected photon from the input port “In” passes through CPBS₁. The transmitted photon component in state $|R\rangle_1$ passes through WFC₁ and arrives at CPBS₈, and the re-

flected photon component in state $|L\rangle_2$ passes through HWP₁ and CPBS₂. After the above process, the state of the hybrid system is changed from $|\Psi_0\rangle = |\psi\rangle_p \otimes |\psi\rangle_{e_1} \otimes |\psi\rangle_{e_2}$ to $|\Psi_1\rangle$, where

$$|\Psi_1\rangle = T^3 \alpha_p |R\rangle_1 (\alpha_{e_1} |\uparrow\rangle + \beta_{e_1} |\downarrow\rangle)_1 (\alpha_{e_2} |\uparrow\rangle + \beta_{e_2} |\downarrow\rangle)_2 + \frac{\beta_p}{\sqrt{2}} [|R\rangle_3 (\alpha_{e_1} |\uparrow\rangle + \beta_{e_1} |\downarrow\rangle)_1 (\alpha_{e_2} |\uparrow\rangle + \beta_{e_2} |\downarrow\rangle)_2 - |L\rangle_4 (\alpha_{e_1} |\uparrow\rangle + \beta_{e_1} |\downarrow\rangle)_1 (\alpha_{e_2} |\uparrow\rangle + \beta_{e_2} |\downarrow\rangle)_2]. \quad (7)$$

For the component of the photon in state $|R\rangle_3$, it passes through WFC₂ and arrives at CPBS₃. For the photon component in state $|L\rangle_4$, it experiences optical elements QWP₁ and P_π in sequence, and then it is transmitted by TR₁ (transmit) for interacting with B₁, where the electron spin in QD₁ is set. In the circuit of B₁, if the photon triggers the single-photon detector, the process of the high-fidelity Toffoli gate is terminated. Otherwise, the process of the gate continues, where the emitting photon component will be reflected by TR₂ (reflect) to path 5 and unites with the component from path 3 to path 6 by CPBS₃. Now, the state of the photon together with the two electron spins evolves into

$$|\Psi_2\rangle = T^3 \alpha_p |R\rangle_1 (\alpha_{e_1} |\uparrow\rangle + \beta_{e_1} |\downarrow\rangle)_1 (\alpha_{e_2} |\uparrow\rangle + \beta_{e_2} |\downarrow\rangle)_2 + \frac{T}{\sqrt{2}} \beta_p [|R\rangle_6 (\alpha_{e_1} |\uparrow\rangle + \beta_{e_1} |\downarrow\rangle)_1 (\alpha_{e_2} |\uparrow\rangle + \beta_{e_2} |\downarrow\rangle)_2 + |L\rangle_6 (\alpha_{e_1} |\uparrow\rangle - \beta_{e_1} |\downarrow\rangle)_1 (\alpha_{e_2} |\uparrow\rangle + \beta_{e_2} |\downarrow\rangle)_2]. \quad (8)$$

Next, after the photon components in path 6 experience the operation performed by HWP₂, CPBS₄ transmits and reflects the photon components to path 7 and path 8 according to the polarization. For the photon component in state $|R\rangle_7$, it passes through WFC₃ and arrives at CPBS₅ directly. For the photon component in state $|L\rangle_8$, it passes through QWP₂ and interacts with B₂. Note that, before and after the interaction between the photon and B₂, two Hadamard operations are performed on the electron spin in QD₂, which is set in B₂. Similarly, if there is a click of the single-photon detector in B₂, the process of the high-fidelity Toffoli gate is terminated. Otherwise, the process continues, and the whole system collapses into the state $|\Psi_3\rangle$, where

$$|\Psi_3\rangle = T^3 \alpha_p |R\rangle_1 (\alpha_{e_1} |\uparrow\rangle + \beta_{e_1} |\downarrow\rangle)_1 (\alpha_{e_2} |\uparrow\rangle + \beta_{e_2} |\downarrow\rangle)_2 + T^2 \beta_p [|R\rangle_7 (\alpha_{e_1} \alpha_{e_2} |\uparrow\uparrow\rangle + \alpha_{e_1} \beta_{e_2} |\uparrow\downarrow\rangle)_1 + |L\rangle_8 (\beta_{e_1} \alpha_{e_2} |\downarrow\downarrow\rangle + \beta_{e_1} \beta_{e_2} |\downarrow\uparrow\rangle)_1]. \quad (9)$$

Then, the photon components in state $|R\rangle_7$ and in state $|L\rangle_8$ unite with each other to path 9 by CPBS₅ for passing through HWP₃ and CPBS₆. By this time, the state of the whole system evolves into $|\Psi_4\rangle$, where

$$|\Psi_4\rangle = T^3 \alpha_p |R\rangle_1 (\alpha_{e_1} |\uparrow\rangle + \beta_{e_1} |\downarrow\rangle)_1 (\alpha_{e_2} |\uparrow\rangle + \beta_{e_2} |\downarrow\rangle)_2 + \frac{T^2}{\sqrt{2}} \beta_p [|R\rangle_{10} (\alpha_{e_1} \alpha_{e_2} |\uparrow\uparrow\rangle + \alpha_{e_1} \beta_{e_2} |\uparrow\downarrow\rangle)_1 + |R\rangle_{10} (\beta_{e_1} \alpha_{e_2} |\downarrow\downarrow\rangle + \beta_{e_1} \beta_{e_2} |\downarrow\uparrow\rangle)_1]. \quad (10)$$

$$+ |L\rangle_{11}(\alpha_{e_1}\alpha_{e_2}|\uparrow\uparrow\rangle + \alpha_{e_1}\beta_{e_2}|\uparrow\downarrow\rangle)_{12} \\ - |L\rangle_{11}(\beta_{e_1}\alpha_{e_2}|\downarrow\downarrow\rangle + \beta_{e_1}\beta_{e_2}|\downarrow\uparrow\rangle)_{12}. \quad (10)$$

Finally, the photon component in state $|R\rangle_{10}$ passes through WFC₄ and arrives at CPBS₇. However, the photon component in state $|L\rangle_{11}$ passes through QWP₃ and TR₁ (reflect) for interacting with B₁ again. After the interaction, if there is a click of the single-photon detector in B₁, the process of the high-fidelity Toffoli gate is terminated. Otherwise, the photon component emitting from B₁ is transmitted by TR₂ (transmit) for uniting with the $|R\rangle_{10}$ component by CPBS₇. After the Hadamard and bit-flip operations performed by HWP₄ and QWP₄ on the photon components in path 13, CPBS₈ lets the photon move out of the circuit, and the final state of the whole system that is composed of the flying photon and the two electron spins in two QDs is obtained as follows:

$$|\Psi_5\rangle = T^3[\alpha_p|R\rangle\alpha_{e_1}|\uparrow\rangle_1(\alpha_{e_2}|\uparrow\rangle + \beta_{e_2}|\downarrow\rangle)_2 \\ + \alpha_p|R\rangle\beta_{e_1}|\downarrow\rangle_1(\alpha_{e_2}|\uparrow\rangle + \beta_{e_2}|\downarrow\rangle)_2 \\ + \beta_p|L\rangle\alpha_{e_1}|\uparrow\rangle_1(\alpha_{e_2}|\uparrow\rangle + \beta_{e_2}|\downarrow\rangle)_2 \\ + \beta_p|L\rangle\beta_{e_1}|\downarrow\rangle_1(\alpha_{e_2}|\downarrow\rangle + \beta_{e_2}|\uparrow\rangle)_2]. \quad (11)$$

By comparing the realistic final state $|\Psi_5\rangle$ with the initial state $|\Psi_0\rangle$, one can see that the state of the target qubit (i.e., the electron spin in QD₂) is flipped only when the control qubits (i.e., the flying photon and the electron spin in QD₁) are in states $|L\rangle$ and $|\downarrow\rangle_1$, respectively. Through further comparing the realistic final state $|\Psi_5\rangle$ with the ideal output state of the Toffoli gate, one can find that there are no error items appearing in state $|\Psi_5\rangle$, that is, in our Toffoli gate, the computation errors which come from the imperfect scattering do not happen. Based on the definition of fidelity $F = |\langle \Psi_r | \Psi_i \rangle|^2$, where $|\Psi_i\rangle$ and $|\Psi_r\rangle$ are the ideal output state and the realistic final state, respectively, one can see that the fidelity of our Toffoli gate approaches unity in the nearly realistic condition. That is, the fidelity of our Toffoli gate is robust to the realistic scattering parameters such as coupling strength, cavity leakage, and frequency difference. Overall, the compact quantum circuit shown in Fig. 2 implements a high-fidelity Toffoli gate on a three-qubit hybrid system.

4. High-fidelity Fredkin gate on a three-qubit hybrid system

A Fredkin gate on a three-qubit hybrid system is used to perform a swap operation on two target qubits (encoded on two electron spins in two QDs) or not, depending on the states of the control qubit (encoded on a flying photon). For obtaining the Fredkin gate without computation errors coming from imperfect scattering process (i.e., obtaining the Fredkin gate with a high fidelity robust to the realistic parameters of the practical scattering), we utilize the optical elements and the basic blocks to construct the quantum circuit, as shown in Fig. 3.

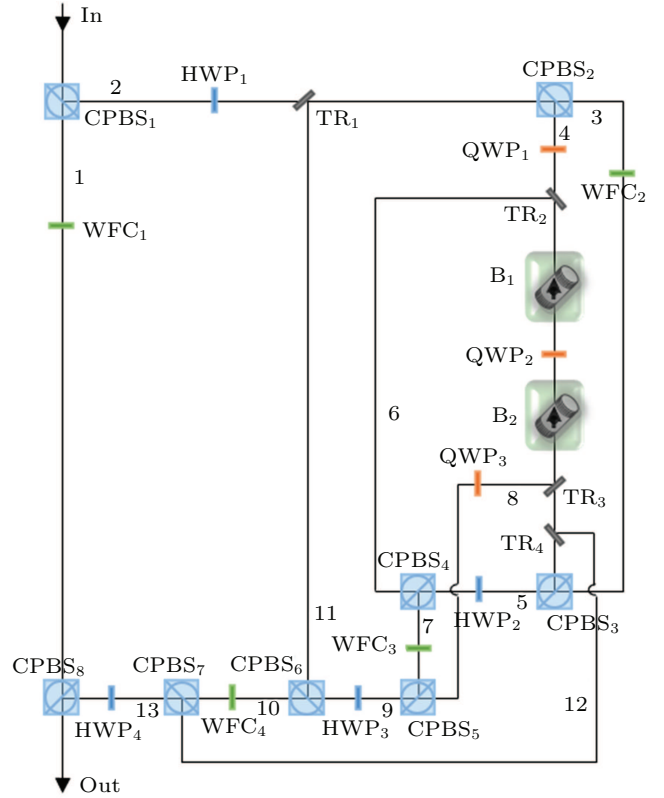


Fig. 3. Schematic diagram for the high-fidelity Fredkin gate on a three-qubit hybrid system. WFC₁ and WFC_{2,3,4} modify the intensity of the incident photon with coefficients T^6 and T^2 , respectively.

Suppose that the control photon and two target electron spins in QD₁ and in QD₂ are prepared in arbitrary normalized states $|\varphi\rangle_p = \alpha_p|R\rangle + \beta_p|L\rangle$, $|\varphi\rangle_{e_1} = \alpha_{e_1}|\uparrow\rangle_1 + \beta_{e_1}|\downarrow\rangle_1$, and $|\varphi\rangle_{e_2} = \alpha_{e_2}|\uparrow\rangle_2 + \beta_{e_2}|\downarrow\rangle_2$, respectively. The Fredkin gate realizes the function that when the control photon is in the state $|L\rangle$, a swap operation is performed on the states of the two target electron spins in QD₁ and QD₂; otherwise, the states of the target electron spins are unchanged. Let us discuss the detailed principle in the following.

First, the photon enters the quantum circuit from the input port “In” and passes through CPBS₁. The right-circularly polarized photon component is transmitted to path 1 for passing through WFC₁ and arriving at CPBS₈, whereas the left-circularly polarized photon component is reflected to path 2, which will successively pass through HWP₁ → TR₁ (transmit) → CPBS₂. After these operations, the state of the hybrid system is changed from $|\Omega\rangle_0 = |\varphi\rangle_p \otimes |\varphi\rangle_{e_1} \otimes |\varphi\rangle_{e_2}$ to $|\Omega\rangle_1$, where

$$|\Omega\rangle_1 = T^6\alpha_p|R\rangle_1(\alpha_{e_1}|\uparrow\rangle + \beta_{e_1}|\downarrow\rangle)_1(\alpha_{e_2}|\uparrow\rangle + \beta_{e_2}|\downarrow\rangle)_2 \\ + \frac{\beta_p}{\sqrt{2}}[|R\rangle_3(\alpha_{e_1}|\uparrow\rangle + \beta_{e_1}|\downarrow\rangle)_1(\alpha_{e_2}|\uparrow\rangle + \beta_{e_2}|\downarrow\rangle)_2 \\ - |L\rangle_4(\alpha_{e_1}|\uparrow\rangle + \beta_{e_1}|\downarrow\rangle)_1(\alpha_{e_2}|\uparrow\rangle + \beta_{e_2}|\downarrow\rangle)_2]. \quad (12)$$

For the photon component in state $|R\rangle_3$, it passes through WFC₂ and arrives at CPBS₃. For the photon component in state $|L\rangle_4$, it experiences operations performed by the optical elements QWP₁ → TR₂ (transmit) → B₁ → QWP₂ → B₂ in

sequence. If either of the single-photon detectors in B_1 or B_2 clicks, the process of the high-fidelity Fredkin gate is terminated. Otherwise, the photon component emitting from B_2 is transmitted by TR_3 (transmit) and TR_4 (transmit) for combining with the photon component in state $|R\rangle_3$ with $CPBS_3$. After the photon components in path 5 pass through HWP_2 , the hybrid system evolves into state $|\Omega\rangle_2$, where

$$|\Omega\rangle_2 = T^6 \alpha_p |R\rangle_1 (\alpha_{e_1} |\uparrow\rangle + \beta_{e_1} |\downarrow\rangle)_1 (\alpha_{e_2} |\uparrow\rangle + \beta_{e_2} |\downarrow\rangle)_2 + T^2 \beta_p [|R\rangle_5 (\alpha_{e_1} \beta_{e_2} |\uparrow\downarrow\rangle + \beta_{e_1} \alpha_{e_2} |\downarrow\uparrow\rangle)_1 + |L\rangle_5 (\alpha_{e_1} \alpha_{e_2} |\uparrow\uparrow\rangle + \beta_{e_1} \beta_{e_2} |\downarrow\downarrow\rangle)_1]. \quad (13)$$

Secondly, $CPBS_4$ reflects the photon component in state $|L\rangle_5$, which subsequently passes through WFC_3 in path 7 and arrives at $CPBS_5$. Meanwhile, $CPBS_4$ transmits the photon component in state $|R\rangle_5$, which is reflected by TR_2 (reflect) to path 4 for experiencing a series of operations performed by $B_1 \rightarrow QWP_2 \rightarrow B_2$ in sequence. Notably, before and after the photon component interacting with B_1 (B_2), Hadamard operations are performed on the electron spin in QD_1 (QD_2). Similarly, if either of the single-photon detectors in B_1 or B_2 clicks, the process of the Fredkin gate is terminated. Otherwise, the photon component emitting from B_2 will be reflected by TR_3 (reflect) to path 8 for passing through QWP_3 and units with the photon component from path 7 by $CPBS_5$. Now, the hybrid system collapses into the state

$$|\Omega\rangle_3 = T^6 \alpha_p |R\rangle_1 (\alpha_{e_1} |\uparrow\rangle + \beta_{e_1} |\downarrow\rangle)_1 (\alpha_{e_2} |\uparrow\rangle + \beta_{e_2} |\downarrow\rangle)_2 + T^4 \beta_p [|R\rangle_9 (\alpha_{e_1} \beta_{e_2} |\downarrow\uparrow\rangle + \beta_{e_1} \alpha_{e_2} |\uparrow\downarrow\rangle)_1 + |L\rangle_9 (\alpha_{e_1} \alpha_{e_2} |\uparrow\uparrow\rangle + \beta_{e_1} \beta_{e_2} |\downarrow\downarrow\rangle)_1]. \quad (14)$$

Thirdly, the photon components emerging in path 9 pass through HWP_3 and $CPBS_6$, which transmits the photon component in state $|R\rangle_9$ to path 10 for passing through WFC_4 and arriving at $CPBS_7$. However, the photon component in state $|L\rangle_9$ is reflected by $CPBS_6$ to path 11, and then it is successively reflected by TR_1 (reflect) and $CPBS_2$ to path 4, in which it experiences the operations performed by $QWP_1 \rightarrow TR_2$ (transmit) $\rightarrow B_1 \rightarrow QWP_2 \rightarrow B_2$ in sequence. Similarly, if either of the two single-photon detectors in B_1 and B_2 clicks, the process of the Fredkin gate is terminated. Otherwise, the photon component emitting from B_2 is transmitted by TR_3 (transmit) and reflected by TR_4 (reflect) to path 12. Then the state of the whole system is changed into

$$|\Omega\rangle_3 = T^6 \alpha_p |R\rangle_1 (\alpha_{e_1} |\uparrow\rangle + \beta_{e_1} |\downarrow\rangle)_1 (\alpha_{e_2} |\uparrow\rangle + \beta_{e_2} |\downarrow\rangle)_2 + \frac{T^6}{\sqrt{2}} \beta_p [|R\rangle_{10} (\alpha_{e_1} \beta_{e_2} |\downarrow\uparrow\rangle + \beta_{e_1} \alpha_{e_2} |\uparrow\downarrow\rangle)_1 + |R\rangle_{10} (\alpha_{e_1} \alpha_{e_2} |\uparrow\uparrow\rangle + \beta_{e_1} \beta_{e_2} |\downarrow\downarrow\rangle)_1 - |L\rangle_{12} (\alpha_{e_1} \beta_{e_2} |\downarrow\uparrow\rangle + \beta_{e_1} \alpha_{e_2} |\uparrow\downarrow\rangle)_1 - |L\rangle_{12} (\alpha_{e_1} \alpha_{e_2} |\uparrow\uparrow\rangle + \beta_{e_1} \beta_{e_2} |\downarrow\downarrow\rangle)_1]. \quad (15)$$

After the photon components in state $|R\rangle_{10}$ and in state $|L\rangle_{12}$ unite with each other by $CPBS_7$ and pass through HWP_4 , $CPBS_8$ performs the last operation which combines the two photon components from path 1 and path 13 to the output port “Out”. The final state of the whole hybrid system is obtained as

$$|\Omega\rangle_4 = T^6 [\alpha_p |R\rangle (\alpha_{e_1} |\uparrow\rangle + \beta_{e_1} |\downarrow\rangle)_1 (\alpha_{e_2} |\uparrow\rangle + \beta_{e_2} |\downarrow\rangle)_2 + \beta_p |L\rangle (\alpha_{e_2} |\uparrow\rangle + \beta_{e_2} |\downarrow\rangle)_1 (\alpha_{e_1} |\uparrow\rangle + \beta_{e_1} |\downarrow\rangle)_2]. \quad (16)$$

From Eq. (16), one can see that, compared with the initial state $|\Omega_0\rangle$, the states of the two target qubits (i.e., the electron spins in QD_1 and QD_2) are swapped when the control qubit (i.e., the flying photon) is in the state $|L\rangle$, whereas they are not swapped when the control qubit is in the state $|R\rangle$. Meanwhile, one can see that there are no error items appearing in the realistic final state $|\Omega\rangle_4$ as described in Eq. (16). That is to say, even though we use practical scattering to construct our Fredkin gate, no computation errors, which come from the imperfect photon scattering process, is happening. Accordingly, the fidelity robust to the realistic scattering parameters is obtained. Overall, the compact quantum circuit shown in Fig. 3 realizes a high-fidelity Fredkin gate based on the practical photon scattering.

5. Discussion

We have presented two schemes for implementing high-fidelity Toffoli gate and Fredkin gate via the practical scattering of a photon off a QD-cavity system. In what follows, we evaluate the performance of the quantum gate, which can be described by fidelity and efficiency. Efficiency is defined as the ratio of the number of the outputting photons to the inputting photons, and the efficiencies of the Toffoli gate and Fredkin gate can be obtained as

$$\eta_T = |T|^6, \quad \eta_F = |T|^{12}, \quad (17)$$

which both vary with the parameters $g/(2\kappa + \kappa_s)$ and κ_s/κ as shown in Fig. 4. The high-quality AlAs/GaAs micropillar cavity with coupling strength as $g/(2\kappa + \kappa_s) = 2.4$ ($g = 80 \mu\text{eV}$, $2\kappa + \kappa_s = 33 \mu\text{eV}$) was reported by Reitzenstein *et al.*,^[97] and the cavity leaky rate $\kappa_s/\kappa = 0.05$ could possibly be achieved as illustrated by Hu *et al.*^[98] For a practical scattering condition with $g/(2\kappa + \kappa_s) = 2.4$ and $\kappa_s/\kappa = 0.05$, the efficiencies of the Toffoli gate and Fredkin gate can be obtained as $\eta_T = 77.77\%$ and $\eta_F = 60.48\%$. It should be pointed out that the efficiency is sacrificed for high fidelity since the possible computation errors are converted into detectable photon losses, which is advantageous for quantum computation.

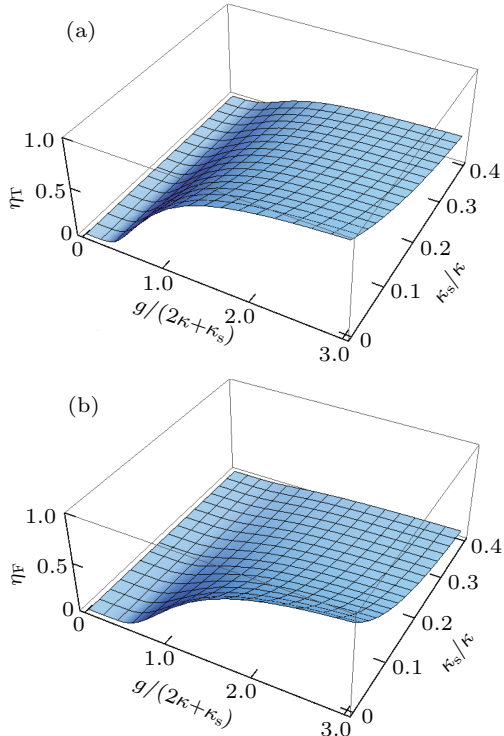


Fig. 4. (a) The efficiency of high-fidelity Toffoli gate vs $g/(2\kappa + \kappa_s)$ and κ_s/κ . (b) The efficiency of high-fidelity Fredkin gate vs $g/(2\kappa + \kappa_s)$ and κ_s/κ . Here, the X^- dipole decay rate $\gamma/\kappa = 0.1$ and the resonant condition $\omega = \omega_c = \omega_{X^-}$ are used.

Fidelity indicates the difference between the realistic final state and the ideal output state. We have shown that compared with the ideal output states, there exist no error items in the realistic final states of the Toffoli gate and the Fredkin gate, even though the practical scattering of a photon off a QD-cavity system is utilized to construct the scheme, as shown in Eqs. (11) and (16). That is to say, the fidelities of these two quantum gates are robust to the realistic scattering parameters, such as the coupling strength $g/(2\kappa + \kappa_s)$, cavity leaky rate κ_s/κ , and the frequency difference $\Delta = \omega - \omega_c$.

In a more generally realistic condition, some other factors which would have effects on the performance should be taken into account. Hu *et al.*^[70] pointed out that the intrinsic electron-spin decoherence in a realistic QD can decrease the fidelity of the photon scattering off the QD-cavity by a factor $[1 + \exp(-\Delta t/T_2^e)]/2$, where Δt is the time interval between incident photons and T_2^e is the electron-spin coherence time. This effect can reduce the fidelity by few percents, since $T_2^e > 3 \mu\text{s}$ can be achieved through spin echo techniques and $\Delta t \sim \text{ns}$ can be achieved in experiment^[56] which can also guarantee the weak excitation approximation.^[70] On the other hand, the fidelity can also be reduced by amount of $[1 - \exp(-\tau/T_2)]$, which is caused by exciton dephasing effect including the optical dephasing and the spin dephasing of X^- . Here, τ is the cavity photon lifetime and T_2 is the exciton coherence time. The optical coherence time can be ten times longer than the cavity photon lifetime,^[99–101] which results in

slight reduction of the fidelity by a few percents. The spin coherence time is at least three orders of magnitude longer than the cavity photon lifetime,^[102–104] therefore it is safe to neglect this kind of dephasing effect. Meanwhile, Hu *et al.*^[70] pointed out that the heavy-light hole mixing and the nuclear spin fluctuations can reduce the fidelity slightly. The mixing can be improved by engineering the shape and the size of QDs or choosing different types of QDs,^[105] and the nuclear spin fluctuations can be effectively suppressed via utilizing spin echo^[55,106] or dynamical decoupling techniques.^[107] Moreover, the influences coming from the optical switch and single-photon detector need to be considered. Our schemes can be heralded by single-photon detectors in basic blocks, and the click of the single-photon detector breaks up the the process of the schemes. If the single-photon detector is perfect enough, no click of the single-photon detector marks the success of the scheme. Therefore, the detectable errors would lower the efficiency of the single-photon detector finitely. The loss, delays, and the destruction on photons of the optical switch would affect the scheme quality. Fortunately, the suitable ultrafast optical switching device has been demonstrated, which exhibits minimal loss, high speed performance, and high contrast without disturbing the quantum state of photons.^[108–110]

In addition, some inevitable experimental imperfections in linear optical elements, such as the balancing of CPBSs and BSs, and imperfections in spin state preparation and manipulation would contribute to affecting the fidelity.^[111]

6. Conclusion

We have proposed two protocols for implementing high-fidelity Toffoli and Fredkin gates for hybrid systems by utilizing the practical scattering of the photon off the QD-cavity system. We convert the undesired computation errors from the imperfect scattering induced by weak coupling strength, cavity side leakage, and frequency difference into the detectable photon loss by single-photon detectors. Therefore, with our schemes, the desired computation results without computation errors of the two gates can be obtained under a nearly realistic condition, robust fidelity with some practical scattering parameters can be guaranteed, and the requirement for high- Q microcavity can be relaxed. Meanwhile, the accomplishment of these two gates requires no auxiliary qubits and the circuits are compact, which further relax the experimental realization. We believe that the present theoretical schemes will be useful for their advantages in the quantum computation.

Acknowledgement

Project supported by the National Natural Science Foundation of China (Grant No. 12004029).

References

[1] Nielsen M A and Chuang I L 2000 *Quantum Computation and Quantum Information* (Cambridge: Cambridge University Press)

[2] Shor P W 1997 *SIAM J. Comput.* **26** 1484

[3] Grover L K 1997 *Phys. Rev. Lett.* **79** 325

[4] Long G L 2001 *Phys. Rev. A* **64** 022307

[5] Reiserer A, Kalb N, Rempe G and Ritter S 2014 *Nature* **508** 237

[6] Tiecke T G, Thompson J D, de Leon N P, Liu L R, Vuletic V and Lukin M D 2014 *Nature* **508** 241

[7] Shi Y Y 2003 *Quantum Inf. Comput.* **3** 84

[8] Fredkin E and Toffoli T 1982 *Int. J. Theor. Phys.* **21** 219

[9] Cory D G, Price M D, Maas W, Knill E, Laflamme R, Zurek W H, Havel T F and Somaroo S S 1998 *Phys. Rev. Lett.* **81** 2152

[10] Dennis E 2001 *Phys. Rev. A* **63** 052314

[11] Knill E, Laflamme R and Milburn G J 2001 *Nature* **409** 46

[12] Duan L M and Kimble H J 2004 *Phys. Rev. Lett.* **92** 127902

[13] Nielsen M A 2004 *Phys. Rev. Lett.* **93** 040503

[14] Gong Y X, Guo G C and Ralph T C 2008 *Phys. Rev. A* **78** 012305

[15] O'Brien J L, Pryde G J, White A G, Ralph T C and Branning D 2003 *Nature* **426** 264

[16] Gasparoni S, Pan J W, Walther P, Rudolph T and Zeilinger A 2004 *Phys. Rev. Lett.* **93** 020504

[17] Nemoto K and Munro W J 2004 *Phys. Rev. Lett.* **93** 250502

[18] Li X Q, Wu Y W, Steel D, Gammon D, Stievater T H, Katzer D S, Park D, Piermarocchi C and Sham L J 2003 *Science* **301** 809

[19] Wei H R and Deng F G 2013 *Opt. Express* **21** 17671

[20] Wang C, Zhang Y, Jiao R Z and Jin G S 2013 *Opt. Express* **21** 19252

[21] Kang Y H, Xia Y and Lu P M 2016 *Quantum Inf. Process.* **15** 4521

[22] Ren B C, Wei H R and Deng F G 2013 *Laser Phys. Lett.* **10** 095202

[23] Wei H R, Liu W Q and Chen N Y 2020 *Ann. Phys. (Berlin)* **532** 1900578

[24] Long G L and Xiao L 2003 *J. Chem. Phys.* **119** 8473

[25] Jones J A, Mosca M and Hansen R H 1998 *Nature* **393** 344

[26] Feng G R, Xu G F and Long G L 2013 *Phys. Rev. Lett.* **110** 190501

[27] Xin T, Hao L, Hou S Y, Feng G R and Long G L 2019 *Sci. China Phys. Mech. Astron.* **62** 960312

[28] Yamamoto T, Pashkin Y A, Astafiev O, Nakamura Y and Tsai J S 2003 *Nature* **425** 941

[29] DiCarlo L, Chow J M, Gambetta J M, Bishop L S, Johnson B R, Schuster D I, Majer J, Blais A, Frunzio L, Girvin S M and Schoelkopf R J 2009 *Nature* **460** 240

[30] Neeley M, Bialczak R C, Lenander M, Lucero E, Mariantoni M, O'Connell A, Sank D, Wang H, Weides M, Wenner J, Yin Y, Yamamoto T, Cleland A N and Martinis J M 2010 *Nature* **467** 570

[31] Romero G, Ballester D, Wang Y M, Scarani V and Solano E 2012 *Phys. Rev. Lett.* **108** 120501

[32] Barends R, Kelly J, Megrant A, Veitia A, Sank D, Jeffrey E, White T C, Mutus J, Fowler A G, Campbell B, Chen Y, Chen Z, Chiaro B, Dunsworth A, Neill C, O'Malley P, Roushan P, Vainsencher A, Wenner J and Korotkov A N 2014 *Nature* **508** 500

[33] Andersen C K and Mølmer K 2015 *Phys. Rev. A* **91** 023828

[34] Loss D and DiVincenzo D P 1998 *Phys. Rev. A* **57** 120

[35] Imamoglu A, Awschalom D D, Burkard G, DiVincenzo D P, Loss D, Sherwin M and Small A 1999 *Phys. Rev. Lett.* **83** 4204

[36] Hu C Y, Munro W J and Rarity J G 2008 *Phys. Rev. B* **78** 125318

[37] Hu C Y, Munro W J, O'Brien J L and Rarity J G 2009 *Phys. Rev. B* **80** 205326

[38] Wei H R and Deng F G 2014 *Opt. Express* **22** 593

[39] van der Sar T, Wang Z H, Blok M S, Bernien H, Taminiau T H, Toyli D M, Lidar D A, Awschalom D D, Hanson R and Dobrovitski V V 2012 *Nature* **484** 82

[40] Wei H R and Deng F G 2013 *Phys. Rev. A* **88** 042323

[41] Cao C, Duan Y W, Chen X, Zhang R, Wang T J and Wang C 2017 *Opt. Express* **25** 16931

[42] Jaksch D, Briegel H J, Cirac J I, Gardiner C W and Zoller P 1999 *Phys. Rev. Lett.* **82** 1975

[43] Jaksch D, Cirac J I, Zoller P, Rolston S L, Côté R and Lukin M D 2000 *Phys. Rev. Lett.* **85** 2208

[44] Isenhower L, Urban E, Zhang X L, Gill A T, Henage T, Johnson T A, Walker T G and Saffman M 2010 *Phys. Rev. Lett.* **104** 010503

[45] Sørensen A S and Mølmer K 2003 *Phys. Rev. Lett.* **91** 097905

[46] Wang H F, Zhu A D and Zhang S 2014 *Opt. Lett.* **39** 1489

[47] Song J, Xia Y and Song H S 2009 *Europhys. Lett.* **87** 50005

[48] Xiao Y F, Lin X M, Gao J, Yang Y, Han Z F and Guo G C 2004 *Phys. Rev. A* **70** 042314

[49] Bonato C, Haupt F, Oemrawsingh S S R, Gudat J, Ding D, vanExter M P and Bouwmeester D 2010 *Phys. Rev. Lett.* **104** 160503

[50] Liang L M and Li C Z 2005 *Phys. Rev. A* **72** 024303

[51] Wei H R and Deng F G 2013 *Phys. Rev. A* **87** 022305

[52] Wang T J, Zhang Y and Wang C 2014 *Laser Phys. Lett.* **11** 025203

[53] Bechler O, Borne A, Rosenblum S, Guendelman G, Mor O E, Netser M, Ohana T, Aqua Z, Drucker N, Finkelstein R, Lovsky Y, Bruch R, Gurovich D, Shafir E and Dayan B 2018 *Nat. Phys.* **14** 996

[54] Song G Z, Guo J L, Liu Q, Wei H R and Long G L 2021 *Phys. Rev. A* **104** 012608

[55] Petta J R, Johnson A C, Taylor J M, Laird E A, Yacoby A, Lukin M D, Marcus C M, Hanson M P and Gossard A C 2005 *Science* **309** 2180

[56] Greilich A, Yakovlev D R, Shabaev A, Efros A L, Yugova I A, Oulton R, Stavarache V, Reuter D, Wieck A and Bayer M 2006 *Science* **313** 341

[57] Elzerman J M, Hanson R, Willems van Beveren L H, Witkamp B, Vandersypen L M K and Kouwenhoven L P 2004 *Nature* **430** 431

[58] Kroutvar M, Ducommun Y, Heiss D, Bichler M, Schuh D, Abstreiter G and Finley J J 2004 *Nature* **432** 81

[59] Atatüre M, Dreiser J, Badolato A, Högele A, Karrai K and Imamoglu A 2006 *Science* **312** 551

[60] Atatüre M, Dreiser J, Badolato A and Imamoglu A 2007 *Nat. Phys.* **3** 101

[61] Berezovsky J, Mikkelsen M H, Stoltz N G, Coldren L A and Awschalom D D 2008 *Science* **320** 349

[62] Press D, Ladd T D, Zhang B Y and Yamamoto Y 2008 *Nature* **456** 218

[63] Gupta J A, Knobel R, Samarth N and Awschalom D D 2001 *Science* **292** 2458

[64] Chen P C, Piermarocchi C, Sham L J, Gammon D and Steel D G 2004 *Phys. Rev. B* **69** 075320

[65] Hanson R, Willems van Beveren L H, Vink I T, Elzerman J M, Naber W J M, Koppens F H L, Kouwenhoven L P and Vandersypen L M K 2005 *Phys. Rev. Lett.* **94** 196802

[66] Yoshie T, Scherer A, Hendrickson J, Khitrova G, Gibbs H M, Rupper G, Ell C, Shchekin O B and Deppe D G 2004 *Nature* **432** 200

[67] Chen H J 2018 *Photonics Res.* **6** 1171

[68] Arnold C, Demory J, Loo V, Lemaître A, Sagnes I, Glazov M, Krebs O, Voisin P, Senellart P and Lanço L 2015 *Nat. Commun.* **6** 6236

[69] Androvitsanea P, Young A B, Schneider C, Maier S, Kamp M, Höfling, Knauer S, Harbord E, Hu C Y, Rarity J G and Oulton R 2016 *Phys. Rev. B* **93** 241409(R)

[70] Hu C Y and Rarity J G 2011 *Phys. Rev. B* **83** 115303

[71] Bennett A J, Lee J P, Ellis D J P, Farrer I, Ritchie D A and Shields A J 2016 *Nat. Nanotechnol.* **11** 857

[72] Sun S, Kim H, Solomon G S and Waks E 2016 *Nat. Nanotechnol.* **11** 539

[73] Li Y, Aolita L, Chang D E and Kwek L C 2012 *Phys. Rev. Lett.* **109** 160504

[74] Cao C, Chen X, Duan Y W, Fan L, Zhang R, Wang T J and Wang C 2016 *Sci. China Phys. Mech. Astron.* **59** 100315

[75] Liu Y T, Wu Y M and Du FF 2022 *Chin. Phys. B* **31** 050303

[76] Borregaard J, Kólmár P, Kessler E M, Sørensen A S and Lukin M D 2015 *Phys. Rev. Lett.* **114** 110502

[77] Li T and Deng F G 2016 *Phys. Rev. A* **94** 062310

[78] Li T and Long G L 2016 *Phys. Rev. A* **94** 022343

[79] Qin W, Wang X, Miranowicz A, Zhong Z and Nori F 2017 *Phys. Rev. A* **96** 012315

[80] Ren B C and Deng F G 2017 *Opt. Express* **25** 10863

[81] Shapira Y, Shaniv R, Manovitz T, Akerman N and Ozeri R 2018 *Phys. Rev. Lett.* **121** 180502

[82] Wang G Y, Li T, Ai Q and Deng F G 2018 *Opt. Express* **26** 23333

[83] Li M and Zhang M 2018 *Opt. Express* **26** 33129

[84] Li M, Lin J Y and Zhang M 2019 *Ann. Phys. (Berlin)* **531** 1800312

[85] Wei H R, Zheng Y B, Hua M and Xu G F 2020 *Appl. Phys. Express* **13** 082007

[86] Xu Y, Chu J, Yuan J H, Qiu J W, Zhou Y X, Zhang L B, Tan X S, Yu Y, Liu S, Li J, Yan F and Yu D P 2020 *Phys. Rev. Lett.* **125** 240503

[87] Han Y H, Cao C, Fan L and Zhang R 2021 *Opt. Express* **29** 20045

[88] Cao C, Han Y H, Zhang L, Fan L, Duan Y W and Zhang R **2019** *Adv. Quantum Technol.* **2** 1900081

[89] Cao C, Zhang L, Han Y H, Yin P P, Fan L, Duan Y W and Zhang R **2020** *Opt. Express* **28** 2857

[90] Fan L and Cao C **2021** *J. Opt. Soc. Am. B* **38** 1593

[91] Du F F, Liu Y T, Shi Z R, Liang Y X, Tang J and Liu J **2019** *Opt. Express* **27** 27046

[92] Walls D F and Milburn G J **1994** *Quantum Optics* (Berlin: Springer-Verlag)

[93] An J H, Feng M and Oh C H **2009** *Phys. Rev. A* **79** 032303

[94] Wang G Y, Ai Q, Deng F G and Ren B C **2020** *Opt. Express* **28** 18693

[95] Reck M and Zeilinger A **1994** *Phys. Rev. Lett.* **73** 58

[96] Ren B C, Du F F and Deng F G **2013** *Phys. Rev. A* **88** 012302

[97] Reitzenstein S, Hofmann C, Gorbunov A, Strauß M, Kwon S H, Schneider C, Löffler A, Höfting S, Kamp M and Forchel A **2007** *Appl. Phys. Lett.* **90** 251109

[98] Hu C, Young A, O'Brien J, Munro W and Rarity J **2008** *Phys. Rev. B* **78** 085307

[99] Borri P, Langbein W, Schneider S, Woggon U, Sellin R L, Ouyang D and Bimberg D **2001** *Phys. Rev. Lett.* **87** 157401

[100] Birkedal D, Leosson K and Hvam J M **2001** *Phys. Rev. Lett.* **87** 227401

[101] Langbein W, Borri P, Woggon U, Stavarache V, Reuter D and Wieck A D **2004** *Phys. Rev. B* **70** 033301

[102] Heiss D, Schaeck S, Huebl H, Bichler M, Abstreiter G, Finley J J, Bulaev D V and Loss D **2007** *Phys. Rev. B* **76** 241306

[103] Gerardot B D, Brunner D, Dalgarno P A, Öhberg P, Seidl S, Kroner M, Karrai K, Stoltz N G, Petroff P M and Warburton R J **2008** *Nature* **451** 441

[104] Brunner D, Gerardot B D, Dalgarno P A, Wüst G, Karrai K, Stoltz N G, Petroff P M and Warburton R J **2009** *Science* **325** 70

[105] Bester G, Nair S and Zunger A **2003** *Phys. Rev. B* **67** 161306

[106] Clark S M, Fu K M C, Zhang Q, Ladd T D, Stanley C and Yamamoto Y **2009** *Phys. Rev. Lett.* **102** 247601

[107] Viola L, Knill E and Lloyd S **1999** *Phys. Rev. Lett.* **82** 2417

[108] Hall M, Altepeter J and Kumar P **2011** *Phys. Rev. Lett.* **106** 053901

[109] Hall M, Altepeter J and Kumar P **2011** *New J. Phys.* **13** 105004

[110] Rambo T M, Altepeter J B and Kumar P **2016** *Phys. Rev. A* **93** 052321

[111] Zhou X J, Liu W Q, Zheng Y B, Wei H R and Du F F **2022** *Ann. Phys. (Berlin)* **534** 2100509